Journal of the Korean Astronomical Society
48: 399 ∼ 412, 2015 December

http://dx.doi.org/10.5303/JKAS.2015.48.6.399
pISSN: 1225-4614 · eISSN: 2288-890X
http://jkas.kas.org

# Study of Milli-Jansky Seyfert Galaxies with Strong Forbidden High-Ionization Lines Using the Very Large Array Survey Images

Dharam V. Lal

National Centre for Radio Astrophysics (NCRA–TIFR), Pune University Campus, Post Box 3, Ganeshkhind P.O., Pune 411007, India; dharam@ncra.tifr.res.in

Received November 30, 2015; accepted December 16, 2015

**Abstract:** We study the radio properties at 1.4 GHz of Seyfert galaxies with strong forbidden high-ionization lines (FHILs), selected from the Sloan Digital Sky Survey – a large-sized sample containing nearly equal proportion of diverse range of Seyfert galaxies showing similar redshift distributions compiled by Gelbord et al. (2009) using the Very Large Array survey images. The radio detection rate is low, 49%, which is lower than the detection rate of several other known Seyfert galaxy samples. These galaxies show low star formation rates and the radio emission is dominated by the active nucleus with ≤10% contribution from thermal emission, and possibly, none show evidence for relativistic beaming. The radio detection rate, distributions of radio power, and correlations between radio power and line luminosities or X-ray luminosity for narrow-line Seyfert 1 (NLS1), Seyfert 1 and Seyfert 2 galaxies are consistent with the predictions of the unified scheme hypothesis. Using correlation between radio and [O III] λ 5007 Å luminosities, we show that ∼8% sample sources are radio-intermediate and the remaining are radio-quiet. There is possibly an ionization stratification associated with clouds on scales of 0.1–1.0 kpc, which have large optical depths at 1.4 GHz, and it seems these clouds are responsible for free–free absorption of radio emission from the core; hence, leading to low radio detection rate for these FHIL-emitting Seyfert galaxies.

**Key words:** galaxies: active — galaxies: jets — galaxies: nuclei — galaxies: Seyfert — galaxies: structure — radio continuum: galaxies

## 1. Introduction

Spiral galaxies, having bright star-like nuclei covering a wide range of ionization, are known as Seyfert galaxies. They are generally classified into type 1 and type 2, which depends only on relative nuclear emission-line widths (Khachikian & Weedman 1974). The Seyfert 2 galaxies have relatively narrow permitted hydrogen lines and narrow forbidden lines, whereas Seyfert 1 galaxies have broad permitted hydrogen lines and narrow forbidden lines. The widths of narrow lines and of broad lines in terms of full width at half maximum (FWHM) are ≈ 300–1,000 km s$^{-1}$ and ≥ 1,000 km s$^{-1}$ for type 2 and type 1, respectively. An orientation based unified scheme is often used in explaining the classification of a Seyfert galaxy, where the Seyfert 2 represent edge-on source and the Seyfert 1 galaxy is its pole-on equivalent (e.g., Antonucci 1993; Urry & Padovani 1995; Deo et al. 2007; Netzer 2015). Observational evidence for and against this unified scheme hypothesis exist on various scales and in all wavebands (see Singh et al. 2013, for a brief summary). In all these studies, sample selection is the key; for example, biases against obscured sources, and biases towards dusty sources are suggested for the Optical-/UV-selected samples; whereas biases towards sources with higher level of nuclear star formation are suggested for the infrared-selected sources (Schmitt et al. 2001; Mason et al. 2012). Similarly, optical-/UV-/X-ray selected flux limited samples, are all likely to have intrinsically more luminous Seyfert 2 galaxies than Seyfert 1 galaxies (Heckman et al. 2005; Wang et al. 2009). In short, issues pertaining to sample selection are key and new efforts to test the unified scheme hypothesis with superior and well-chosen samples continue to be made (Lal et al. 2011; Urry & Padovani 1995, and see also Section 2.2).

This paper tests the validity and limitations of the unified scheme hypothesis for Seyfert galaxies. Here, we present results for a Seyfert galaxy sample defined by Gelbord et al. (2009, hereafter GMW09), using Very Large Array (VLA) survey images. This large sample contains a diverse types of Seyfert galaxies. Below, we first explain classifications of Seyfert galaxies (Section 2.1) and give a brief description of the sample (Section 2.2). We use the radio maps from Faint Images of the Radio Sky at Twenty–Centimeters (FIRST; Becker et al. 1995) and NRAO VLA Sky Survey (NVSS; Condon et al. 1998) for the sample objects (Section 3), and interpret our results (Section 4) and their implications on the unified scheme hypothesis (Section 5). Finally, we summarize our conclusions in Section 6.

Following GMW09, we also adopt the same cosmological parameters from *Wilkinson Microwave Anisotropy Probe*. Hence, distance-dependent quantities are calculated assuming $H_0$ = 71 km s$^{-1}$ Mpc$^{-1}$, $\Omega_m$ = 0.27, and $\Omega_\Lambda$ = 0.73 (Spergel et al. 2003). When archive ra-

Corresponding author: D. V. Lal

dio data is available at other frequencies, we determine radio spectral index, $\alpha$ which we define in the sense that $S_\nu \propto \nu^\alpha$, where $S_\nu$ is the flux density and $\nu$ is the frequency. All coordinates mentioned below are for J2000 epoch.

## 2. BACKGROUND

### 2.1. Classifications of Seyfert Galaxies

In addition to Seyfert galaxies of type 1 and type 2; Osterbrock (1981) and Osterbrock & Pogge (1985) introduced additional fractional classifications; these appear to have a mix of properties from both types, as the broad component of H$\beta$ becomes weaker as compared to the narrower component, the Seyfert type changes from 1.2 $\rightarrow$ 1.5 $\rightarrow$ 1.8 $\rightarrow$ 1.9. Seyfert 1.2 and 1.5 galaxies have composite spectra, with both broad and narrow components easily recognizable and the former have broad component being stronger than narrow component, whereas the latter have both components that are comparable. In Seyfert 1.8 and 1.9 galaxies, in addition to the narrow components, very weak but recognizable broad components of H$\beta$ and H$\alpha$, or of H$\alpha$ alone, respectively are present (Osterbrock 1981). In terms of the unified scheme hypothesis these intermediate Seyfert types are thought to lie at a varying angles between pole-on and edge-on views, with Seyfert 1.2 galaxies being close to pole-on, whereas Seyfert 1.9 galaxies being close to edge-on. Osterbrock & Pogge (1985) proposed yet another type of Seyfert galaxies, the narrow-line Seyfert 1 (NLS1) galaxies (Valencia et al. 2012). These objects have permitted line-widths much smaller than typical Seyfert 1 galaxies. However, they differ from Seyfert 2 galaxies, in the sense that optical spectra of NLS1 galaxies show several characteristics normally associated with Seyfert 1 galaxies, such as [O III]/H$\beta$ ratios of less than 3, permitted lines are broader than forbidden lines, and blends of lines such as Fe II or [Fe VII] or [Fe X]. Again, in the unified scheme frame-work, NLS1 galaxies could be sources with views very close to pole-on (Urry & Padovani 1995).

### 2.2. FHIL-Emitting Seyfert Galaxy Sample

Our goal is to study the radio properties of Seyfert galaxies and their implications on the unified scheme hypothesis, and we use Seyfert galaxies listed in GMW09, with strong forbidden high-ionization line (FHIL) emission. This sample contains a diverse types of Seyfert galaxies, including NLS1 galaxies. It has

- 12 NLS1,
- 14 type 1.0,
- 16 type 1.5,
- 2 type 1.9, and
- 18 type 2.0 Seyfert galaxies.

Almost all known nearby, $z \lesssim 0.1$ Seyfert galaxy samples, e.g., the bright Seyfert galaxies sample (Giuricin et. al. 1990), the CfA Seyfert sample (Huchra & Burg 1992), the 12 $\mu$m Seyfert sample (Rush et al. 1993; Hunt & Malkan 1999), the far-infrared selected Seyfert galaxy sample (Roy et al. 1994), the matched Seyfert sample (Lal et al. 2011), etc. rarely have NLS1 galaxies in them and do not have appropriate proportion of Seyfert types discussed above. Other FHIL-emitting samples of Seyfert galaxies in the literature (e.g., De Robertis & Osterbrock 1984; Erkens et al. 1997; Murayama & Taniguchi 1998; Veilleux 1998; Nagao et al. 2000) are all relatively small and heterogeneous. Instead, the GMW09 sample of Seyfert galaxies with strong FHILs is one of the largest containing nearly equal proportion of diverse Seyfert types and hence, by far the most homogeneous to date. In order to discuss differences between NLS1, Seyfert 1 and Seyfert 2 galaxies and its implications on the unified scheme hypothesis, we henceforth address Seyfert 1.0 and 1.5, and Seyfert 1.9 and 2.0 as Seyfert 1, and Seyfert 2 galaxies, respectively. Note that GMW09 found one galaxy with an unusual spectrum that is not Seyfert-like (object 45, spectral type "gal" in GMW09), which was neither included by GMW09 nor it is included in the rest of this paper. We also do not include radio galaxy 3C 234 (object 22, spectral type "Seyfert 1.9"), though it was included by GMW09, because it is a radio-loud active galactic nucleus (AGN; Laing et al. 1983). One another source (object 53, spectral type "NLS1") is not covered by the FIRST survey and is not detected in NVSS image; this too is excluded.

Our final sample consists of 61 (from parent list of 64) Seyfert galaxies. All these 61 objects have measured [Fe X], [Fe VII] and [O III] fluxes and among these 59% (36/61) objects have measured [Fe XI] fluxes, which is twice as many as compared to earlier samples in the literature. The mean redshifts and their dispersions for individual sub-classes of Seyfert galaxies are,

- NLS1: $0.0764 \pm 0.0313$,
- Seyfert 1.0: $0.0962 \pm 0.0612$,
- Seyfert 1.5: $0.1061 \pm 0.0701$,
- Seyfert 1.9: $0.0877 \pm 0.0341$, and
- Seyfert 2.0: $0.0694 \pm 0.0382$.

These means are based on redshifts defined from the observed wavelengths of the [S II] doublet. It seems that the Seyfert 1.0 and 1.5 galaxies in the sample are farther set of objects with respect to the mean redshift for the sample $0.0869 \pm 0.0532$ possibly due to the bias mentioned above. However, much of it is due to three outlier objects, ID-12 (spectral type 1.0), and ID-16 and ID-28 (spectral type 1.5), which are only objects with $z > 0.2$ in the sample; and excluding these objects, the means are $0.0840 \pm 0.0426$ and $0.0843 \pm 0.0391$ for Seyfert 1.0 and Seyfert 1.5, respectively. Barring this, the mean redshifts and their distributions (see Figure 4, GMW09) for diverse types of Seyfert galaxies agree among themselves. In addition, the median redshifts of all Seyfert types also agree. Therefore, apart from only possible bias, bias against Seyfert 1 galaxies with the broadest permitted lines and any FHIL-emitting sources dominated by lines with lower ionization potentials, presence of which is unclear (GMW09), these Seyfert sub-classes do not differ in redshift distribution. We, thus use this

**Table 1**
Map parameters for the extended sources from the FHIL-emitting Seyfert galaxy sample

| Object | Restoring beam | peak (mJy beam$^{-1}$) | r.m.s. | Contour levels (× r.m.s.) | l.a.s. |
|---|---|---|---|---|---|
| SDSS J082930.59+081238.1 | 6.4″×5.4″ | 2.624 | 0.11 | −3, 3, 4, 6, 8, 10 | 6″ |
| SDSS J092343.00+225432.6 | 5.4″×5.4″ | 5.516 | 0.08 | −3, 3, 4, 8, 12, 16, 20, 24, 32, 40, 48, 56 | 17″ |
| SDSS J110704.52+320630.0 | 5.4″×5.4″ | 2.666 | 0.10 | −3, 3, 4, 8, 12, 16, 20, 24 | 6″ |
| SDSS J115704.84+524903.7 | 5.4″×5.4″ | 2.142 | 0.10 | −3, 3, 4, 6, 8, 10 | 12″ |
| SDSS J122930.41+384620.7 | 5.4″×5.4″ | 1.349 | 0.10 | −3, 3, 4, 6, 8, 10, 12 | 8″ |
| SDSS J134607.71+332210.8 | 5.4″×5.4″ | 0.785 | 0.10 | −3, 3, 4, 6 | ≃ 5″ |
| SDSS J153552.40+575409.5 | 5.4″×5.4″ | 4.620 | 0.09 | −3, 3, 4, 8, 10, 12, 16, 20, 24, 32, 40, 48 | 11″ |
| SDSS J220233.85−073225.0 | 6.4″×5.4″ | 1.296 | 0.09 | −3, 3, 4, 8, 10, 12 | 18″ |

sample containing diverse types of Seyfert galaxies with FHIL features to study the radio properties and its implications on the unified scheme hypothesis.

## 3. DATA

Our earlier effort of investigating radio properties of type 2 SDSS quasars (Lal & Ho 2010) yielded a detection rate of 59% (35/59) at 8.4 GHz (X-band) survey. This detection rate was essentially identical to that obtained from FIRST survey images at 1.4 GHz with 5″ resolution, which observed 56 out of the 59 sources in our sample and detected 35 (63%), even though the sensitivity of FIRST survey is nearly an order of magnitude lower than that of our X-band survey (Lal & Ho 2010). Furthermore, the sensitivity of NVSS survey images at 1.4 GHz with 45″ resolution is ∼0.45 mJy beam$^{-1}$ (Condon et al. 1998), a factor of three lower than the FIRST survey images and surprisingly the detection rate was again identical. Since, the sample of 61 Seyfert galaxies with FHIL-emitting features also come from SDSS, we believe that deeper new observations may not be necessary to understand basic radio properties. We therefore use FIRST survey images (at 1.4 GHz, ∼5″ resolution) together with NVSS images (at 1.4 GHz, ∼45″ resolution), and archive VLA data, when available along with published optical and X-ray (GMW09) data extensively to draw our conclusions.

## 4. RESULTS

### 4.1. Maps and Source Parameters

Galaxies were considered detected if the peak flux density $S^{1.4\,\mathrm{GHz}}_{\mathrm{Peak}} > 5 \times$ r.m.s. noise, where the noise of each map was determined from a source–free region. In total 30 sources from the sample of 61 were detected, of which eight were resolved. The radio images of eight sources showing extended, resolved structures, are shown in Figure 1. These source images are arranged in the order of increasing R.A., and their restoring beams (with position angles = 0°), root-mean-squared (r.m.s.) values and contour levels in the maps are given in Table 1. The ratio of the peak surface brightness and the r.m.s. noise, or the dynamic range for the FIRST survey, and the NVSS images are between ∼5 and 66, and ∼6 and 43, respectively. For the undetected sources, the flux density or its upper limit is equal to 5 × r.m.s. The sizes (major and minor axes) and elongation direction (position angle) of the detected components/sources were determined by fitting two-dimensional Gaussians to each detected source and deconvolving those Gaussians from the synthesized beams using Astronomical Image Processing System (AIPS[1]) task JMFIT. The data for the sources with complex morphologies, the flux densities were found from integration over the maps covering the source using AIPS task TVSTAT.

A summary of derived radio parameters from the FIRST survey images, along with optical parameters is given in Table 2, together with Seyfert galaxy types in the following order: NLS1, Seyfert 1.0, 1.5, 1.9, and 2.0, which are further arranged in the order of increasing R.A. The individual columns are: (1) Object name; (2) ID Number as defined by GMW09; (3) spectral classification; (4) redshift from the observed wavelength of the [S II] doublet; (5) luminosity distance[2]; (6) r.m.s. noise in the map; (7) peak flux density; (8) integrated flux density; (9) deconvolved (half maximum) size of the source (major and minor axes); (10) largest linear size (l.l.s.); (11) comments on the source structure; and (12) integrated flux density as determined from the NVSS image.

For each object in Table 2, we have classified the radio structure into following categories (Ulvestad & Wilson 1984; Ulvestad & Ho 2001): "U" (unresolved), "S" (slightly resolved), "L" (linear, usually core–jet or double), and "E" (extended); where slightly resolved and extended sources are those whose deconvolved size is ≥ 0.5 times the synthesized beam width (Ulvestad & Ho 2001; Lal & Ho 2010). Whenever we obtain zero arcsec as the deconvolved size in any one dimension, we ascribe "U" (unresolved) status to the object.

### 4.2. Notes on Extended Sources

There are 8 out of the 30 confirmed detections which are extended.

*SDSS J082930.59+081238.1* — This source appears extended in the FIRST image and is classified as diffuse with faint extended emission. The low-surface brightness feature toward the northeast seen at 1.4 GHz is

[1] http://www.aips.nrao.edu
[2] computed using Ned Wright's online cosmology calculator http://www.astro.ucla.edu/$\sim$wright/CosmoCalc.html

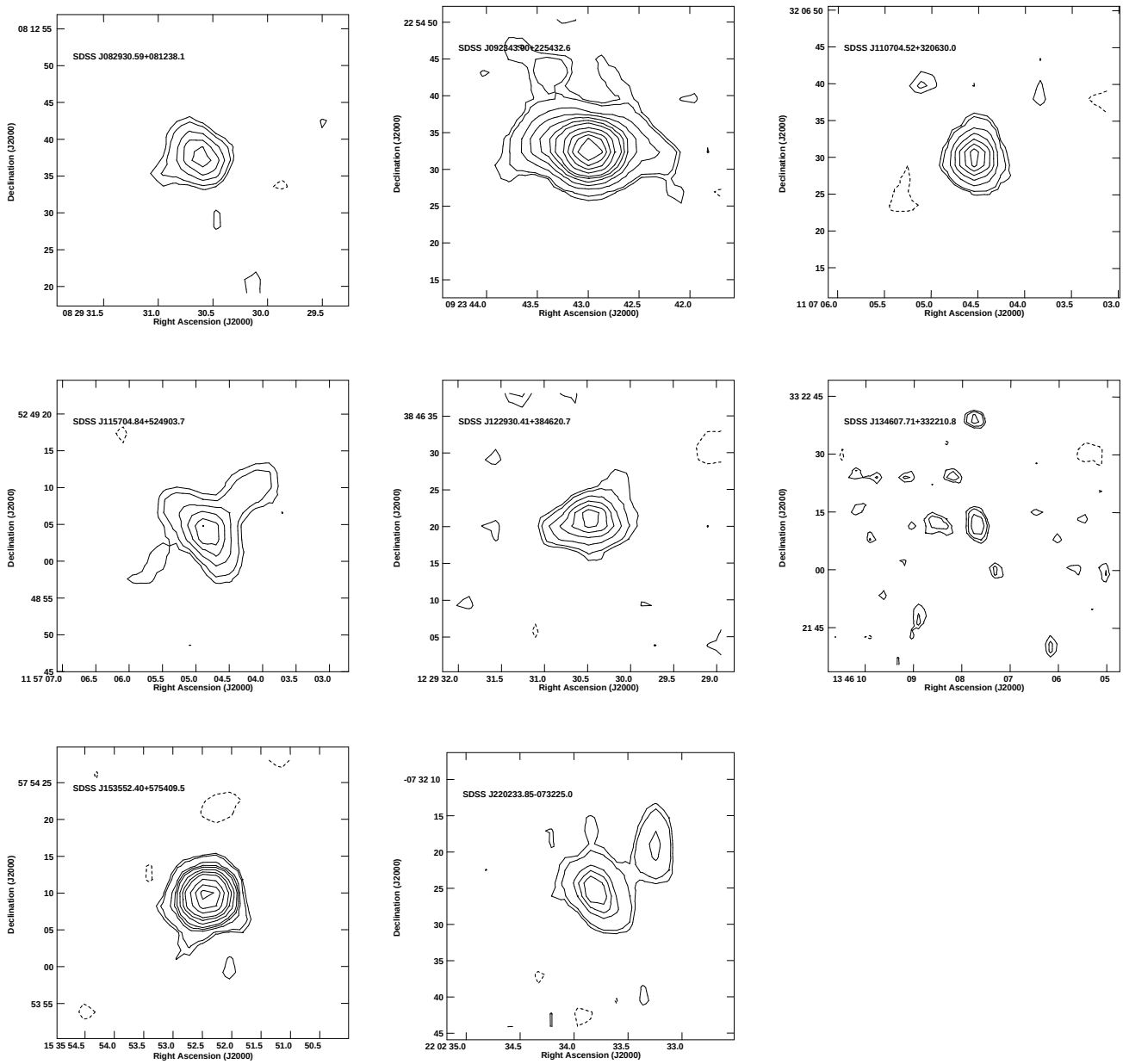


**Figure 1.** VLA *B*-array configuration, 1.4 GHz images with 5″ resolution (FIRST: Becker et al. 1995) of selected FHIL-emitting Seyfert galaxies from SDSS showing extended radio structures. The fields are centered on the optical positions given by GMW09. The contour levels and surface brightness peaks are listed in Table1.

possibly a jet.

*SDSS J092343.00+225432.6* — The radio core is unresolved but the source appears to have east–west elongation. The low-surface brightness contours suggest the source to be amorphous and is classified as an extended morphology.

*SDSS J110704.52+320630.0* — A marginal case of core-jet (Kharb et al. 2010) morphology. The faint jet is seen as emanating from the core along the northern direction.

*SDSS J115704.84+524903.7* — The source is resolved, with typical core–jet morphology.

*SDSS J122930.41+384620.7* — The source is marginally resolved with an extension along east.

*SDSS J134607.71+332210.8* — The low-surface brightness contours at $3\sigma$–$5\sigma$ levels suggest that the source is possibly a diffuse, with extended structure. Assuming the structure at the phase-center and the extended feature adjacent to it on the east to be real, the source is likely to be of core–jet morphology.

*SDSS J153552.40+575409.5* — This object is also classified as Mrk 290 (PG1534+580) at $z = 0.0296$ (NED) in the literature. The radio core is slightly resolved at 1.4 GHz. An image using archive VLA

*A*-array configuration data at 5.0 GHz (project-code AF0402, observe-date 2003-Jun-17) shows the source to be unresolved. The integrated spectral index using FIRST survey image and this archive data, $\alpha_{1.4\,\mathrm{GHz}}^{5.0\,\mathrm{GHz}} = -0.73 \pm 0.04$, typical of many other Seyfert galaxies (Lal et al. 2011).

*SDSS J220233.85−073225.0* — This source has a double-lobed extended morphology at 1.4 GHz. It is the southeast radio lobe, which is associated with the optical position. Hence, it is possible that radio core is slightly resolved showing a core–jet morphology.

## 5. Discussion

### 5.1. The Radio Properties

#### 5.1.1. Radio Detection Rate

Of the 61 FHIL-emitting Seyfert galaxies in the sample, 30 (49%) have been detected down to the FIRST survey r.m.s. sensitivity limit of 0.15 mJy beam$^{-1}$ (Becker et al. 1995). This detection rate further lowers, 34% (21/61) if we instead consider NVSS data. Furthermore, this detection rate is:

1. lower than the detection rate of type 2 SDSS quasars sample (Lal & Ho 2010, median redshift = 0.427), ∼59% (35/59) and 63% (35/56) using X-band images and using FIRST survey images, respectively;
2. lower than the detection rate of complete sample of local Seyfert galaxies (Panessa & Giroletti 2013, median redshift = 0.003): 74% (17 of 23, milliarcsec-scale resolution) and 100% (23 of 23, VLA, arcsec-scale resolutions);
3. lower than the detection rate of matched sample of Seyfert galaxies (Lal et al. 2011, median redshift = 0.019): 100% (20 of 20; both, milliarcsec-scale and arcsec-scale resolutions);
4. lower than the detection rate of extended 12 $\mu$m Seyfert galaxy sample (Rush et al. 1993; Thean et al. 2000, median redshift = 0.008): 86% (75 of 87; VLA *A*-array configuration, sub-arcsec-scale resolutions);
5. lower than the detection rate of CfA Seyfert galaxy sample (Huchra & Burg 1992; Kukula et al. 1995, median redshift = 0.0141): 81% (39 of 48; VLA *A*-array configuration, sub-arcsec-scale resolutions) and 88% (42 of 48; VLA *C*-array configuration, arcsec-scale resolutions);
6. lower than the detection rate of bright Seyfert galaxies sample (Giuricin et. al. 1990, median redshift = 0.009): 90%;
7. (nearly) similar to the detection rate of far-infrared selected Seyfert galaxy sample: ∼39% (Roy et al. 1994, median redshift = 0.031).

Note that barring type 2 SDSS quasar sample (Lal & Ho 2010), all other Seyfert galaxy samples are nearby (redshift $\lesssim 0.03$), and except radio observations of two Seyfert galaxy samples, Roy et al. (1994) and (Panessa & Giroletti 2013), which are at higher angular resolutions, the radio data of all other samples are at similar, arcsecond-scale resolutions. Among these nearby Seyfert galaxy samples, the detection rates of FHIL-emitting Seyfert galaxy and far-infrared selected samples are similar. Looking more closely only at the detected sources, the sample size of 21 objects; namely,

- three (out of 11) NLS1,
- four (out of 14) Seyfert 1.0,
- four (out of 16) Seyfert 1.5,
- one (out of 2) Seyfert 1.9 and
- nine (out of 18) Seyfert 2.0.

Thus, the detection rates of NLS1, Seyfert 1 and Seyfert 2 galaxies are $0.25 \pm 0.16$, $0.27 \pm 0.11$, and $0.50 \pm 0.07$, respectively. Alternatively, the radio detection rate of compact radio structure for NLS1, Seyfert 1 and Seyfert 2 is consistent with the unified scheme hypothesis.

Ulvestad et al. (1981), Whittle et al. (1986), Evans et al. (1991) and Falcke et al. (1998) noted that compact radio emission is closely associated with individual narrow-line region clouds, and Roy et al. (1994, and see also Norris et al. 1992) first invoked a model that free–free absorption by these clouds may explain the low detection rate in FHIL-emitting Seyfert galaxies. In particular, when observing Seyfert galaxies showing very low radio emission from the nucleus, either (i) the narrow-line region or (ii) the individual narrow-line region clouds would absorb radio emission; i.e., if the optical depths are above unity due to free–free absorption then either the narrow-line region or the individual narrow-line clouds will block our view of the core and we would not detect it in radio band. Although this model involve optical depth effects in the narrow-line region, its geometry and filling factor, it reconciles our low radio detection rate. Furthermore, in this model, the narrow-line region clouds would become optically thin at higher frequencies and optically thick at further lower frequencies (Norris et al. 1992). So new radio observations at a sufficiently high frequencies should find higher detection rates and similarly, at sufficiently low frequencies should find lower detection rates, which is a possible test if free–free absorption by these clouds is indeed responsible for the low detection rate at 1.4 GHz for the FHIL-emitting Seyfert galaxies in the sample.

#### 5.1.2. Projected Linear Sizes

Twenty-two of 30 (∼73%) detected objects are classified as "U" or "S", unresolved or slightly resolved and the radio emission in these is largely from the central active nucleus. This result shows that a significant fraction of Seyfert galaxies do not have double/triple radio sources, instead they have unresolved structures on a scale of several hundred parsecs to a few kiloparsecs. The double radio sources that have been found in Seyfert galaxies generally have angular separations smaller than the resolution of the present data (Kukula et al. 1995; Thean et al. 2000; Lal et al. 2004). Although the exact number must await high-resolution

**Table 2**
Summary of radio properties derived from FIRST survey images together with ID number (GMW09), Seyfert type, redshift and luminosity distance.

| Object | ID | Class | $z_{[\mathrm{S\,II}]}$ | $D_L$ (Mpc) | r.m.s. (mJy beam$^{-1}$) | $S^{\mathrm{Peak}}_{1.4\,\mathrm{GHz}}$ | $S^{\mathrm{Int.}}_{1.4\,\mathrm{GHz}}$ (mJy) | $\theta_{\mathrm{maj}} \times \theta_{\mathrm{min}}$ (arcsec$^2$) | l.l.s. (kpc) | Notes | $S_{1.4\,\mathrm{GHz}}$ (mJy) |
|---|---|---|---|---|---|---|---|---|---|---|---|
| (1) | (2) | (3) | (4) | (5) | (6) | (7) | (8) | (9) | (10) | (11) | (12) |
| SDSS J001852.47+010758.5 | 2 | NLS1 | 0.0583 | 257 | 0.142 | | <0.71 | | | | <2.25 |
| SDSS J092343.00+225432.6 | 20 | NLS1 | 0.0330 | 143 | 0.126 | 5.15 | 9.29 | 6.71 × 2.87 | 11.1 | L+E | 9.55 |
| SDSS J102235.15+022930.5 | 24 | NLS1 | 0.0701 | 312 | 0.138 | | <0.69 | | | | <2.25 |
| SDSS J103438.60+393828.3 | 25 | NLS1 | 0.0435 | 190 | 0.154 | 3.98 | 5.94 | 1.65 × 1.43 | | U | 24.19 |
| SDSS J110243.20+385152.6 | 27 | NLS1 | 0.1186 | 546 | 0.152 | | <0.76 | | | | <2.25 |
| SDSS J120932.94+322429.3 | 40 | NLS1 | 0.1303 | 605 | 0.143 | | <0.72 | | | | <2.25 |
| SDSS J131135.66+142447.2 | 46 | NLS1 | 0.1140 | 524 | 0.140 | | <0.70 | | | | <2.25 |
| SDSS J131957.07+523533.8 | 50 | NLS1 | 0.0922 | 417 | 0.138 | 3.05 | 2.72 | | | U | 3.15 |
| SDSS J161844.85+253907.7 | 59 | NLS1 | 0.0479 | 210 | 0.144 | | <0.72 | | | | <2.25 |
| SDSS J205822.14−065004.4 | 61 | NLS1 | 0.0740 | 331 | 0.139 | | <0.70 | | | | <2.25 |
| SDSS J220233.85−073225.0 | 62 | NLS1 | 0.0594 | 263 | 0.150 | 1.45 | 2.36 | 6.71 × 2.48 | 20.4 | L | <2.25 |
| SDSS J082930.59+081238.1 | 9 | S1.0 | 0.1295 | 601 | 0.144 | 1.51 | 2.32 | 4.37 × 3.50 | 13.7 | E | <2.25 |
| SDSS J083045.41+450235.9 | 11 | S1.0 | 0.1825 | 876 | 0.133 | | <0.67 | | | | <2.25 |
| SDSS J083658.91+442602.4 | 12 | S1.0 | 0.2544 | 1275 | 0.156 | 9.39 | 10.25 | 2.12 × 0.99 | | S | 6.08 |
| SDSS J084622.54+031322.2 | 14 | S1.0 | 0.1070 | 489 | 0.136 | | <0.68 | | | | <2.25 |
| SDSS J110756.55+474434.8 | 30 | S1.0 | 0.0727 | 324 | 0.135 | | <0.68 | | | | <2.25 |
| SDSS J112602.46+343448.2 | 33 | S1.0 | 0.0910 | 411 | 0.139 | | <0.70 | | | | <2.25 |
| SDSS J120422.15−012203.3 | 38 | S1.0 | 0.0834 | 375 | 0.148 | | <0.74 | | | | <2.25 |
| SDSS J121044.28+382010.3 | 41 | S1.0 | 0.0230 | 99 | 0.138 | 5.66 | 5.88 | 1.98 × 0.00 | | U | 7.14 |
| SDSS J131305.69−021039.3 | 47 | S1.0 | 0.0838 | 377 | 0.155 | | <0.78 | | | | <2.25 |
| SDSS J134607.71+332210.8 | 52 | S1.0 | 0.0838 | 377 | 0.130 | 1.11 | 1.41 | 5.81 × 0.50 | 7.8 | E | 2.52 |
| SDSS J143452.46+483942.8 | 54 | S1.0 | 0.0365 | 159 | 0.133 | | <0.67 | | | | <2.25 |
| SDSS J153552.40+575409.5 | 56 | S1.0 | 0.0304 | 131 | 0.146 | 5.11 | 5.32 | 1.15 × 1.05 | 6.6 | E | 4.31 |
| SDSS J161301.63+371714.9 | 58 | S1.0 | 0.0695 | 309 | 0.138 | | <0.69 | | | | <2.25 |
| SDSS J221542.30−003609.8 | 63 | S1.0 | 0.0994 | 452 | 0.135 | 1.55 | 1.62 | 2.33 × 0.00 | | U | <2.25 |
| SDSS J073126.69+452217.5 | 4 | S1.5 | 0.0921 | 417 | 0.128 | 2.75 | 2.68 | 1.67 × 0.00 | | U | 2.50 |
| SDSS J083045.37+340532.1 | 10 | S1.5 | 0.0624 | 276 | 0.141 | | <0.71 | | | | <2.25 |
| SDSS J085740.86+350321.7 | 16 | S1.5 | 0.2752 | 1395 | 0.141 | | <0.71 | | | | <2.25 |
| SDSS J091715.00+280828.2 | 18 | S1.5 | 0.1045 | 477 | 0.139 | | <0.70 | | | | <2.25 |
| SDSS J091825.79+005058.4 | 19 | S1.5 | 0.0871 | 393 | 0.145 | | <0.73 | | | | <2.25 |
| SDSS J094204.79+234106.9 | 21 | S1.5 | 0.0215 | 93 | 0.135 | 5.78 | 5.91 | 1.27 × 0.00 | | U | 5.52 |
| SDSS J101718.26+291434.1 | 23 | S1.5 | 0.0492 | 216 | 0.141 | | <0.71 | | | | <2.25 |
| SDSS J105519.54+402717.5 | 26 | S1.5 | 0.1201 | 554 | 0.132 | | <0.66 | | | | <2.25 |
| SDSS J110704.52+320630.0 | 28 | S1.5 | 0.2425 | 1207 | 0.145 | 3.03 | 2.82 | 1.86 × 0.80 | 22.7 | E | <2.25 |
| SDSS J110716.49+131829.5 | 29 | S1.5 | 0.1848 | 889 | 0.139 | | <0.70 | | | | <2.25 |
| SDSS J115226.30+151727.6 | 36 | S1.5 | 0.1126 | 517 | 0.146 | | <0.73 | | | | <2.25 |
| SDSS J122903.50+294646.1 | 42 | S1.5 | 0.0821 | 369 | 0.129 | | <0.65 | | | | <2.25 |
| SDSS J123149.08+390530.2 | 44 | S1.5 | 0.0683 | 304 | 0.150 | 2.19 | 2.31 | 3.31 × 0.00 | | U | 2.54 |
| SDSS J131348.96+365358.0 | 48 | S1.5 | 0.0670 | 298 | 0.143 | | <0.72 | | | | <2.25 |
| SDSS J163501.46+305412.1 | 60 | S1.5 | 0.0543 | 239 | 0.117 | 2.63 | 2.67 | 1.48 × 0.00 | | U | 3.53 |
| SDSS J235654.30−101605.5 | 64 | S1.5 | 0.0740 | 331 | 0.151 | 1.95 | 1.61 | 1.34 × 0.00 | | U | <2.25 |
| SDSS J001852.47+010758.5 | 1 | S1.9 | 0.0640 | 284 | 0.102 | | <0.51 | | | | <2.25 |
| SDSS J112602.46+343448.2 | 32 | S1.9 | 0.1114 | 511 | 0.145 | 3.64 | 3.81 | 2.56 × 0.00 | | U | 4.88 |
| SDSS J023301.24+002515.0 | 3 | S2.0 | 0.0224 | 96 | 0.095 | 3.89 | 3.98 | 1.68 × 0.00 | | U | 6.02 |
| SDSS J073638.86+435316.5 | 5 | S2.0 | 0.1140 | 524 | 0.135 | 4.59 | 4.26 | 0.54 × 0.00 | | U | 2.97 |
| SDSS J073650.08+391955.2 | 6 | S2.0 | 0.1163 | 535 | 0.131 | 8.13 | 8.65 | 1.75 × 0.86 | | S | 8.82 |
| SDSS J080707.18+361400.5 | 7 | S2.0 | 0.0324 | 140 | 0.140 | 0.71 | 0.71 | 0.54 × 0.50 | | U | 4.35 |
| SDSS J081153.16+414820.0 | 8 | S2.0 | 0.0999 | 454 | 0.131 | | <0.66 | | | | <2.25 |
| SDSS J084215.30+402533.3 | 13 | S2.0 | 0.0553 | 244 | 0.152 | 1.68 | 1.43 | | | U | <2.25 |
| SDSS J085332.22+210533.7 | 15 | S2.0 | 0.0719 | 321 | 0.137 | | <0.69 | | | | <2.25 |
| SDSS J085810.64+312136.3 | 17 | S2.0 | 0.1389 | 649 | 0.141 | 2.20 | 2.05 | 1.52 × 0.00 | | U | <2.10 |
| SDSS J110929.10+284129.2 | 31 | S2.0 | 0.0329 | 143 | 0.149 | | <0.75 | | | | <2.25 |
| SDSS J113917.17+283946.9 | 34 | S2.0 | 0.0234 | 101 | 0.153 | | <0.77 | | | | <2.25 |
| SDSS J114216.88+140359.7 | 35 | S2.0 | 0.0208 | 89 | 0.135 | 1.55 | 1.84 | 3.18 × 1.17 | | S | <2.25 |
| SDSS J115704.84+524903.7 | 37 | S2.0 | 0.0356 | 155 | 0.144 | 1.19 | 4.22 | 8.73 × 8.53 | 8.4 | S+L | 2.81 |
| SDSS J120735.06−001550.3 | 39 | S2.0 | 0.1104 | 506 | 0.138 | | <0.69 | | | | <2.25 |
| SDSS J122930.41+384620.7 | 43 | S2.0 | 0.1024 | 467 | 0.141 | 1.53 | 2.90 | 7.42 × 2.71 | 14.9 | E | 3.35 |
| SDSS J131639.75+445235.1 | 49 | S2.0 | 0.0911 | 412 | 0.135 | 4.23 | 4.53 | 2.05 × 0.36 | | S | 5.68 |
| SDSS J132346.00+610400.2 | 51 | S2.0 | 0.0715 | 319 | 0.151 | 9.16 | 9.01 | 1.17 × 0.00 | | U | 19.49 |
| SDSS J153222.32+233325.0 | 55 | S2.0 | 0.0465 | 204 | 0.162 | 1.10 | 0.98 | 2.42 × 0.00 | | U | <2.25 |
| SDSS J160948.21+043452.9 | 57 | S2.0 | 0.0643 | 285 | 0.149 | 4.27 | 4.75 | 2.41 × 0.74 | | S | 3.89 |

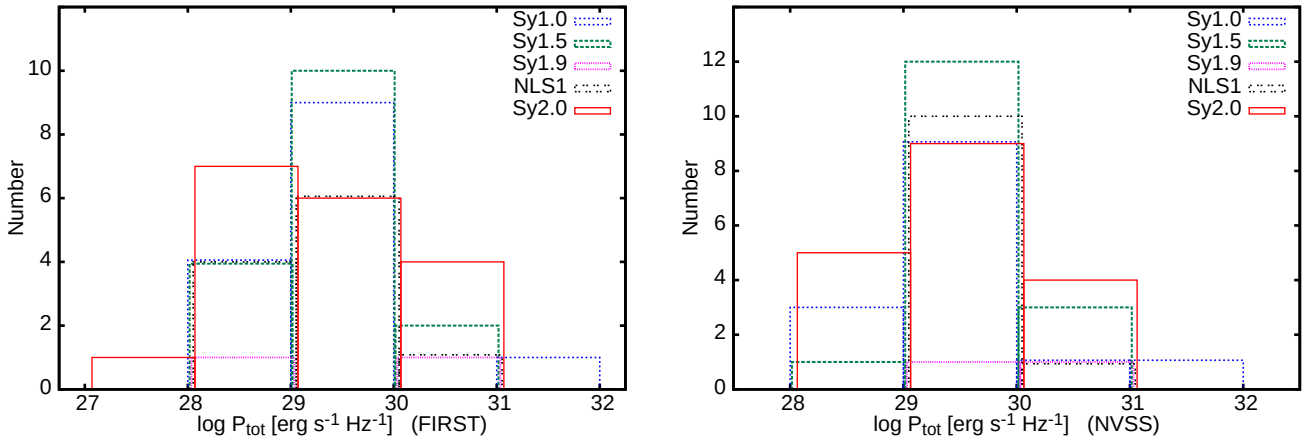


**Figure 2.** Histograms showing distributions of total detected radio luminosity (erg s$^{-1}$ Hz$^{-1}$) for the FHIL-emitting Seyfert galaxies from SDSS at 1.4 GHz using VLA *B*-array (left panel, FIRST: Becker et al. 1995) and the radio luminosity (erg s$^{-1}$ Hz$^{-1}$) at 1.4 GHz using VLA *D*-array (right panel, NVSS: Condon et al. 1998). The undetected sources are not explicitly denoted, they all lie at the lower end of the luminosity, and the bins widths are chosen large enough to incorporate upper limits. Line colours and styles are: NLS1 = black, Seyfert 1.0 = blue, Seyfert 1.5: dark-green, Seyfert 1.9 = magenta, and Seyfert 2.0 = red. The overlapping lines are marginally shifted with respect to each other for clarity.

radio maps of the complete FHIL-emitting Seyfert sample, eight (out of detected 30 = 27%) sources (Figure 1) have marginally extended, about a few kiloparsec scale to a few tens of kiloparsec scale structures. The largest projected linear sizes (l.l.s.), determined from largest-angular-sizes (l.a.s.) listed in Table 1, for eight extended sources shown in Figure 1 corresponding to the $3\sigma$ contour level of the 1.4 GHz maps are listed in Table 2.

Clearly Seyfert 1 and NLS1 galaxies have larger range in projected linear sizes as compared to Seyfert 2 galaxies. Unfortunately with only eight sources, three Seyfert 1, three NLS1 and two Seyfert 2, this is small number statistics. The statistical test[3] gives a poor significance level of 0.25 that the distribution of projected linear sizes of NLS1, Seyfert 1 and Seyfert 2 galaxies are same. Higher-resolution observations are therefore needed to resolve the FIRST survey images into structures with physical sizes less than a kiloparsec, as often seen in nearby Seyfert galaxies (e.g., Kukula et al. 1995; Thean et al. 2000; Lal et al. 2004). These resolved morphologies would provide improved statistics and test the distribution of projected linear sizes at a higher significance level.

### 5.1.3. *Kiloparsec-Scale Radio Luminosities*

Figure 2 shows the distribution of the radio luminosity detected on 5″-scales (FIRST images) and 45″-scales (NVSS images) for all Seyfert sub-classes. Radio luminosities for our sample sources are *K*-corrected, rest-frame values determined from observed flux densities at 1.4 GHz and corresponding luminosity distances (Lal & Ho 2010). Since majority (22 of the 30 confirmed detections) of the sources are unresolved and correspond to core emission, we assume a typical spectral index, $\alpha$ = +0.5 from cores of Seyfert galaxies (Kellermann & Owen 1988). We have also chosen the radio luminosity bin widths sufficiently larger than the r.m.s. noise in the maps to account for upper limits for undetected sources, which are not explicitly denoted in Figure 2. Although non-detections lie in the luminosity-bins corresponding to the low end of radio powers in both panels, the distribution of radio powers at 1.4 GHz is continuous, showing no separation between the detected and the non-detected objects. Furthermore, changing the radio luminosity bin size does not make the distribution bimodal (or multimodal). This suggests that the detected and undetected sources from the FHIL-emitting Seyfert galaxy sample irrespective of Seyfert class denote a single population as a whole.

In addition, the radio power distributions are not significant different between NLS1 galaxies, Seyfert 1 galaxies and Seyfert 2 galaxies. The K–S test gives a significance level of 0.026 or better that the distribution of Seyfert 1 along with NLS1 galaxies and Seyfert 2 galaxies are same for the FIRST and NVSS data. Thus, we conclude that the radio power distributions of Seyfert galaxy types are similar and are consistent with the expectations of the unified scheme.

### 5.1.4. *Nature of Radio Emission*

Baum & Heckman (1989) and Rawlings & Saunders (1991) showed that a correlation exists between the radio luminosity at 5 GHz and the [O III] $\lambda$ 5007 Å narrow-line luminosity. Figure 3 illustrates the distribution of integrated radio power (at 5 GHz) versus [O III] luminosity for the large, heterogeneous sample of AGNs compiled by Xu et al. (1999), after correcting for the cosmology. The data for FHIL-emitting Seyfert galaxies come from 1.4 GHz; and to be consistent with Xu et al. (1999), we converted these measurements to 5 GHz

[3]Since, we are dealing with small number statistics, we use instead Mann–Whitney U test, a non-parametric statistical hypothesis test for small sample sizes (Siegel & Castellan 1981).

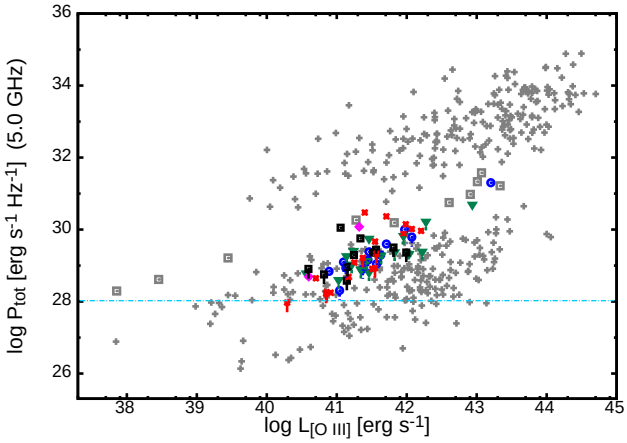


**Figure 3.** Correlation between radio power and [O III] $\lambda$ 5007 Å luminosity. The grey colour plus symbols come from the sample of Xu et al. (1999), with the grey colour squares representing their radio-intermediate sources. The point colours and styles are: NLS1 = black squares, Seyfert 1.0 = blue circles, Seyfert 1.5: dark-green triangles, Seyfert 1.9 = magenta diamonds, and Seyfert 2.0 = red stars. Upper limits are marked with downward-pointing lines. The dashed-dotted line shows the expected radio luminosity at 5 GHz predicted from star formation rate (see Section 5.3).

assuming a flat spectrum spectral index of $\alpha = 0$ and determine the monochromatic power. These monochromatic powers change at the most by a factor of 12%, if instead we assume a slightly inverted or steep spectra (see also Section 5.1.3) and it does not change our interpretations below. Note that we have computed [O III] luminosities using combined fluxes of [O III] core and [O III] wing components (supplementary material: Table A4, Column 8; GMW09). It is clear that AGNs separate into the two families of radio-loud and radio-quiet AGNs with a significant gap between them; i.e., the radio luminosities are different by a factor of $10^3$–$10^4$ between the two groups at a given [O III] luminosity. All the objects in FHIL-emitting Seyfert galaxy sample are of radio-quiet nature, with ∼8% that lie in between the two families of radio-loud and radio-quiet AGNs, also called radio-intermediate AGNs. It is not surprising that all the non-detected sources are radio-quiet. Linear fits to the FHIL-emitting Seyfert galaxy sample excluding the radio-intermediate objects yield

$$\log L_{5\ \mathrm{GHz}} = (0.45 \pm 0.11) \log L_{[\mathrm{O\,III}]} + (5.6 \pm 0.9),$$

which is consistent within error bars with the linear fit by Xu et al. (excluding the radio-intermediate objects; 1999) obtained for the radio-quiet AGNs.

Furthermore, assuming 50% of the flux density detected in the FIRST survey images is also detected at milliarcsec-scales (Lal et al. 2011), the inferred brightness temperature, $T_{\mathrm{B}} \geq 5 \times 10^8$ K for our sample objects, which is again typical of Seyfert galaxies (Broderick & Fender 2011).

#### *5.1.5. Relativistic Beaming*

In radio galaxies, one-sided structures are often associated with relativistic jets and the jet to counter-jet ratios are used to obtain quantitative estimates of relativistic beaming. Here, unfortunately a large fraction of sources are non-detected (∼51% in FIRST and ∼67% in NVSS survey images) and a majority of the rest of the detected sources are unresolved (22 objects out of 30). The FIRST survey images probes structures on scales smaller than the NVSS survey images (see Section 3). Therefore, we assume any difference of the emissions between NVSS and FIRST images as extended emission, which is not Doppler boosted; and instead, if beaming is present, the emission detected in FIRST image would possibly be Doppler boosted (Lal et al. 2011). Hence, the ratio of the possibly boosted and the extended radio flux densities, or the $R$-parameter could be used here to investigate relativistic beaming. Since a majority of sources are not detected, we focus only on the detected sources (see also Section 5.1.1). The ratio of flux density for these detected (20 of 61) sources in both, FIRST and NVSS survey images is close to 1.0 with mean and median being 1.06±0.04 and 1.02, respectively. Clearly, much higher resolution, scales of milli-arcsecond would be required to address relativistic beaming. Additionally, the use of $R$-parameter as measure of relativistic beaming comes with a caveat. Lal et al. (2011) have shown that Seyfert galaxies show radio variability and the FIRST and the NVSS data for the FHIL-emitting Seyfert sample are not simultaneous. Therefore, here we have made an assumption that these sample objects do not show radio variability (see also Mundell et al. 2009).

Additionally, Falcke et al. (1996) showed that Lorentz factors of $\gamma = 2$–$4$ in radio-quiet AGNs are sufficient to boost the radio emission into the radio-intermediate regime or into the radio-loud regime. Five objects from FHIL-emitting Seyfert galaxy sample are of radio-intermediate kind:

- one (out of 11) NLS1,
- one (out of 14) Seyfert 1.0,
- one (out of two) Seyfert 1.9 and
- two (out of 18) Seyfert 2.0.

Although this is a small number statistics, majority are non-type 1 Seyfert galaxies, and it is well known that Seyfert 2 galaxies being edge-on counterparts of beamed population, which are not expected to show relativistic beaming. Therefore, it is possible that FHIL-emitting Seyfert galaxy sample are radio-quiet and there is no evidence of relativistic beaming consistent with the predictions of unified scheme hypothesis, which is further supported by other Seyfert galaxy samples (Lal et al. 2011).

### 5.2. Correlations between Radio and Line Luminosities

In Figure 4, we plot correlations between radio power and luminosities of [Fe X] (top-left panel), [Fe XI] (top-right panel), [Fe VII] (middle-left panel), [O III]

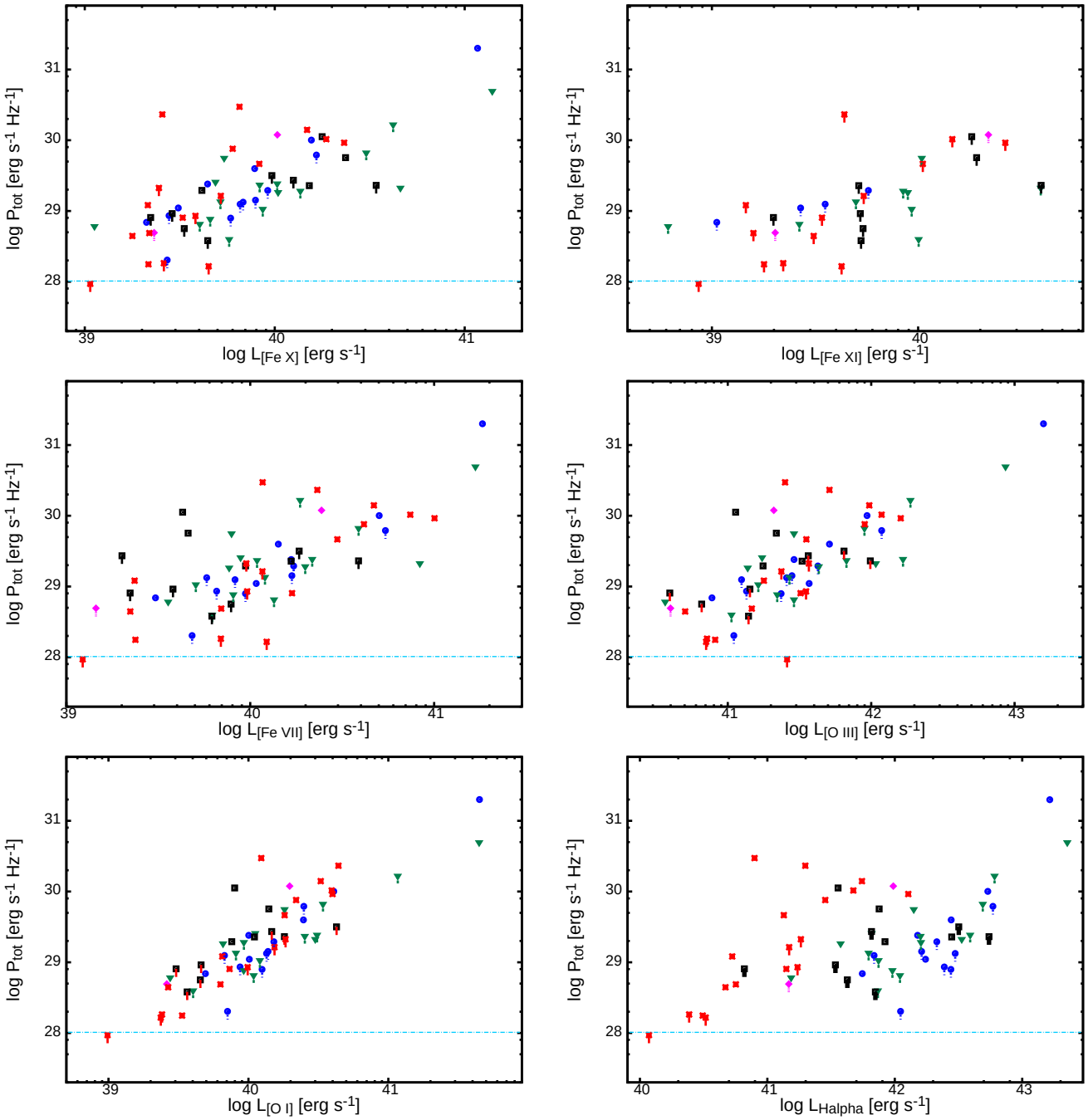


**Figure 4.** Radio power at 1.4 GHz from VLA *B*-array configuration versus luminosities of [Fe X], [Fe XI], [Fe VII], [O III], [O I], and $H_\alpha$. The point colours and styles are: NLS1 = black squares, Seyfert 1.0 = blue circles, Seyfert 1.5: dark-green triangles, Seyfert 1.9 = magenta diamonds, and Seyfert 2.0 = red stars. Upper limits are marked with downward-pointing lines. The dashed-dotted line shows the expected radio luminosity at 5 GHz predicted from star formation rate (see Section 5.3). Error bars (given in Tables A1–A7: supplementary material, GMW09, are not shown, since they are typically ∼2 times the size of the downward-pointing lines.

(middle-right panel), [O I] (bottom-left panel), and $H_\alpha$ (bottom-right panel. [O III] and $H_\alpha$ line luminosities correspond to combined core and wing components and combined narrow and broad $H_\alpha$ model components, respectively (GMW09). In Section 2.1, we discussed inherent biases in the sample and hence possible difference between NLS1, Seyfert 1 and Seyfert 2 galaxies are seen in $H_\alpha$ luminosity, X-ray luminosity, and ratio of [Fe X] and [Fe VII] lines. Barring, correlation between radio power and $H_\alpha$ luminosity, X-ray luminosity and ratio of [Fe X] and [Fe VII] lines, which we discuss below (Section 5.2.1, 5.2.2, 5.2.3, respectively), none suggest that the distribution of NLS1, Seyfert 1 and Seyfert 2 galaxies are dissimilar. We therefore find no observa-

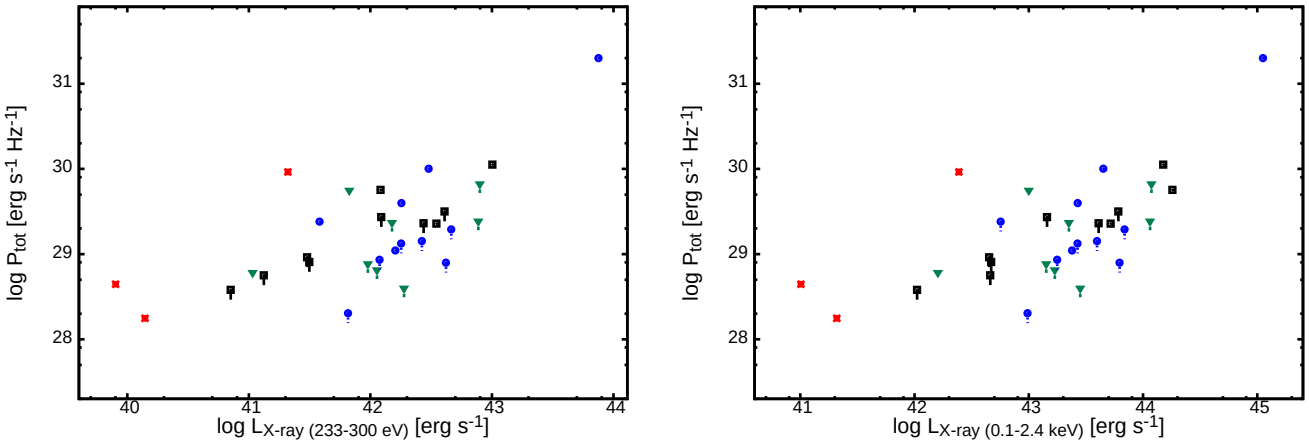


**Figure 5.** Radio power at 1.4 GHz from VLA *B*-array configuration versus luminosities of the soft X-ray band (233–300 eV) and in the hard X-ray band (0.1–2.4 keV). We use softer spectrum ($\Gamma = 3.0$) in the soft X-ray band and harder spectrum ($\Gamma = 1.5$) in the hard X-ray band (GMW09) for NLS1 and Seyfert 1 galaxies with the assumption that they have a softer spectrum in the soft X-ray band and harder spectrum in the hard X-ray band. Whereas Seyfert 2 galaxies have harder spectrum in both soft as well as hard X-ray bands. Point colours and styles are as in Figure 4, and error bars are smaller than the size of the downward-pointing lines.

tional evidence against the unified scheme hypothesis. The K–S test gives a significance level of 0.031 or better that the Seyfert types, Seyfert 1 galaxies along with NLS1 galaxies and Seyfert 2 galaxies are drawn from the same parent population, and there is no significant differences between Seyfert 1 galaxies along with NLS1 galaxies and Seyfert 2 galaxies, based on the distributions of [Fe X], [Fe XI], [Fe VII], [O III], and [O I], which was also independently concluded by GMW09.

Below we discuss those cases where we clearly see segregation between the Seyfert types and their implications on the unified scheme hypothesis.

#### 5.2.1. *Radio and $H_\alpha$ Luminosities*

The radio luminosity versus $H_\alpha$ luminosity correlation plot in Figure 4 (bottom-right panel) show that, both types of Seyfert galaxies have similar radio powers, but Seyfert 2 galaxies have systematically lower $H_\alpha$ luminosity than Seyfert 1 galaxies along with NLS1 galaxies. the latter is because the broad component of $H_\alpha$ in Seyfert 2 galaxies is obscured by the obscuring torus and is always not detected, which is more evident in Figure A2b (from supplementary material) of GMW09. Since the sample is selected on FHIL emission, lines with ionization potential $\gtrsim$100 eV (GMW09), their radio emission is expected to have similar distributions of radio powers within the framework of unified scheme hypothesis. This is indeed the case, i.e., both types of Seyfert galaxies have similar radio powers, consistent with the predictions of unified scheme.

#### 5.2.2. *Radio and X-ray Luminosities*

There are only 32 sample sources with *ROSAT* detections, of which only three are Seyfert 2 galaxies, which on average have lower X-ray luminosities but their radio powers are similar to rest of the sample sources. In Figure 5, we show the correlation between radio and soft X-ray luminosities fitted to Seyfert galaxy populations. Unfortunately, *Chandra*/*XMM-Newton* data do not exist for the sample. Seyfert 1 along with NLS1 galaxies and Seyfert 2 galaxies are known to have, on average, steeper soft X-ray spectra and flatter hard X-ray spectra, respectively (Kruper et al. 1990; Mas-Hesse et al. 1994; Boller 2000; Dadina 2008). Here, we used single uniform photon index, $\Gamma = 1.5$ as well as steeper photon index ($\Gamma = 3.0$) data from GMW09 for Seyfert 1 along with NLS1 galaxies to convert *ROSAT* count rates to fluxes (GMW09; Cappi et al. 2006; Dadina 2008). We find that the same correlation function applies between radio and soft X-ray luminosities for all types of Seyfert galaxies with no systematic differences between them. We therefore conclude that there is no difference between radio luminosities of NLS1, Seyfert 1 and Seyfert 2 galaxies, consistent with unified scheme.

#### 5.2.3. *Radio Luminosity, and Ratio of [Fe X] and [Fe VII] Lines*

Differences between the two types of Seyfert galaxies for the ratio of [Fe X] and [Fe VII] provide evidence that in Seyfert 2 galaxies there exist partially obscured [Fe X] emission and hence low ratio of these two lines (GMW09). This is consistent within the stratified wind model framework discussed below (Section 5.3), that the [Fe X] is emitted on size scales that is comparable to the size of the dusty molecular torus, and hence obscuration may be important. As shown in Figure 6, NLS1 galaxies, Seyfert 1 galaxies and Seyfert 2 galaxies show difference in the ratio of [Fe X] and [Fe VII] which are possibly because of (i) absorption of the [Fe X] or (ii) different ionizing continuum (GMW09), where the latter is perhaps due to the bias in the sample. Briefly, in Seyfert 1 galaxies, the line width of the [Fe X] line profiles is broader, and the ratios of [Fe X] and [Fe VII] tend to be higher, whereas it is in opposite sense for the

Seyfert 2 galaxies (GMW09). These facts suggest that [Fe X]-emitting clouds lie close to the radio core and in certain lines of sights, some fraction of the [Fe X] flux (i.e., the broad component) may be hidden by the obscuring torus (GMW09). Hence, there is possibly an excess of ionizing photons from active nucleus and we expect an over-production of [Fe X] or the higher ratio of [Fe X] and [Fe VII] in the NLS1 galaxies and also in the Seyfert 1 galaxies, whereas this would again be in opposite sense for Seyfert 2 galaxies due to the obscured view of active nucleus by the obscuring torus. These are in line with the expectations of the unified scheme hypothesis. Hence, in Figure 6, we find all types of Seyfert galaxies to have similar radio powers, but the Seyfert 2 galaxies on average have less [Fe X] power per unit of [Fe VII] power than the Seyfert 1 galaxies or NLS1 galaxies, which is again consistent with the predictions of unified scheme.

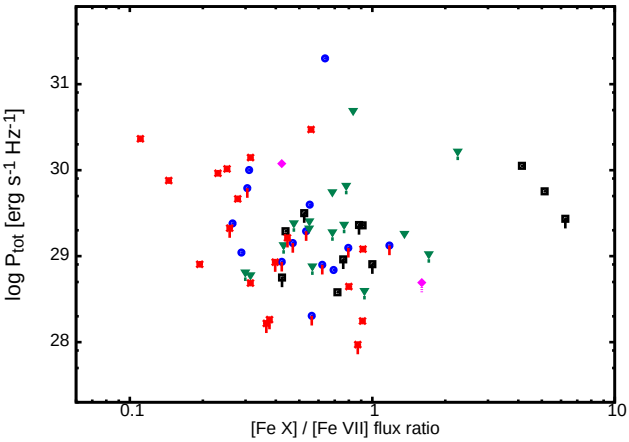


**Figure 6.** Radio power at 1.4 GHz from VLA *B*-array configuration versus [Fe X]/[Fe VII] flux ratio. Point colours and styles are as in Figure 4, and error bars are smaller than the size of the downward-pointing lines.

### 5.3. Starburst vs. AGN Nature of FHIL-Emitting Seyfert Nuclei

We first investigate if the radio emission from 8% radio-intermediate sources in the sample been enhanced due to intense star formation. Quantitatively, the mean radio power of radio-intermediate sources, $P^{\rm tot}_{1.4\,\rm GHz} \simeq 8.5 \times 10^{30}$ erg s$^{-1}$ Hz$^{-1}$ implying a star formation rate (SFR) of $\sim$ 220 $M_\odot\,{\rm yr}^{-1}$ for stars massive enough to form supernovae, i.e., $M \geq 5M_\odot$. Mainieri et al. (2005); Vignali et al. (2009) and Rosario et al. (2012) showed that such high rates of star formation are seen in high-$z$ AGNs, but they are more than the SFR inferred for (i) typical nearby Seyfert galaxies (Alonso-Herrero et al. 2013) by an order of magnitude (Lal et al. 2011), and also for (ii) the most luminous AGNs in the SDSS (Liu et al. 2009). Therefore, it seems that the enhanced radio emission in radio-intermediate sources as compared to radio-quiet sources in the sample is unlikely to be due to intense star formation.

Secondly, the radio spectra of most Seyfert galaxies are known to be steep power laws near 1.4 GHz, $<\alpha>$ $\sim$0.8 (Lal et al. 2011) indicating that the radio flux densities at this frequency are dominated by non-thermal emission. However, the strong optical emission lines imply the presence of ionized gas that could contribute significant thermal emission at frequencies $\geq$1.4 GHz. It is thus important to compare the expected thermal emission and the total radio flux densities observed from Seyfert galaxies in the sample. We now test and demonstrate that both, radio-quiet and radio-intermediate Seyfert galaxies in the sample have low-levels of expected star formation rates, lower than the limits that is needed to account for the observed radio emission. Following Ho (2005, 2008) and also Lal & Ho (2010), the [O II]-derived SFRs are estimated to be $\sim$0.2–10 $M_\odot\,{\rm yr}^{-1}$, with a mean ($\approx$ median) value of $\sim$0.6 $M_\odot\,{\rm yr}^{-1}$ for the Seyfert galaxies in the sample; we use the ratios of ionisation potentials between [O I], [O II] and [O III] emission lines and [O I] and [O III] fluxes, and thereby determine [O II] fluxes. Using Equation 6 of Bell (2003), the predicted radio emission from SFR is $\sim 1.1 \times 10^{28}$ erg s$^{-1}$ Hz$^{-1}$ at 1.4 GHz, which is at least an order of magnitude less than the mean radio luminosity of the sample sources (Figure 3 and 4). Alternatively, assuming all lines of sight through the broad line region are optically thick in the radio, an upper limit to the thermal emission at the mean distance of $\sim$400 Mpc for objects in the sample gives a flux density of $\lesssim$ 0.004 mJy, quite undetectable for typical values of densities of protons and electrons, $n_{\rm p} = n_{\rm e} \simeq 10^9$ cm$^{-3}$ in broad line clouds, of size $\simeq$ 0.1 pc having a temperature $\simeq$ 1.5 $\times 10^4$ K (Koski 1978), a filling factor $\simeq 10^{-4}$ (Ulvestad et al. 1981), and the H$\beta$ luminosity equal to the [O III] $\lambda$ 5007 Å luminosity of $10^{42}$ erg s$^{-1}$ (Ulvestad et al. 1981). On similar lines we calculate radio power $\lesssim 10^{27}$ erg s$^{-1}$ Hz$^{-1}$, using canonical $n_{\rm e} \simeq 10^3$ cm$^{-3}$, temperature $\simeq$ 1.5 $\times 10^4$ K, filling factor $\simeq$ a few times $10^{-2}$ for narrow line clouds of size $\simeq$ 0.1–1.0 kpc at mean distance for objects in the sample. Clearly, it is the narrow line region that has relatively larger thermal emission contribution to the observed radio emission as compared to the broad line region. But the derived thermal contributions at 1.4 GHz are small, at a level of 10% or less of the observed flux density for objects in the FHIL-emitting Seyfert galaxy sample. Also, Gu et al. (2006) used the observed emission-line ratios along with population synthesis models and concluded that although there is a contribution of starbursts to the nuclear emission in a radio-quiet Seyfert galaxies, the contribution of the hidden active nucleus always dominates. Their conclusion compares well for the FHIL-emitting sources studied here.

Finally, in the light of a stratified wind model, first proposed by Osterbrock (1991), outflowing photoionized clouds produce [Fe XI], [Fe X], [Fe VII] and possibly [O III] (GMW09), with high-ionization lines are produced preferentially at small distances from the core, while low-ionization lines are preferentially produced at larger radii. More specifically [Fe XI]- and [Fe X]-emitting clouds lie closest to the radio core and are

on the scale of broad-line region or of obscuring torus, [Fe VII]-emitting clouds are more extended and may approach the scale of narrow-line region, and finally [O III]- and [O II]-emitting clouds, which do not show a velocity shift with respect to [S II] (GMW09), lie farthest from the radio core and more likely are the decelerated part of the stratified wind outflow model (Colbert et al. 1996a,b). If this model is correct, we expect to find a strong correlation between emission-line shifts and ionization potential of the line-emitting species; implying density and ionization stratification (Komossa et al. 2008). Such correlations were indeed reported by GMW09 for some of the ion species. Thus, there is a ionization stratification associated with clouds, and possibly clouds on scales of narrow-line region, which have relatively the least amount of ionization stratification, have large optical depths at 1.4 GHz. These clouds are responsible for free–free absorption of radio emission from the core, leading to inferred low radio detection rate irrespective of Seyfert types, which is consistent with orientation based unified scheme hypothesis.

## 6. CONCLUSIONS AND FUTURE DIRECTIONS

This paper presents radio properties of a sample of 61 sources containing a diverse range of Seyfert galaxies. This is one of the largest, homogeneous samples of Seyfert galaxies with strong FHIL emission selected from the SDSS to date (GMW09). Here we used high-resolution FIRST data (5″ resolution images, Becker et al. 1995) along with low-resolution NVSS radio data (45″ resolution images, Condon et al. 1998), both at 1.4 GHz. Our main results are:

1. Our detection rate of 49% at 1.4 GHz is lower than many other Seyfert galaxy samples, except far-infrared selected sample compiled by Roy et al. (1994).
2. A high fraction (76%) of compact cores are seen within confirmed detected sources. The radio emission within these compact cores is confined to physical sizes $\lesssim$8 kpc. The remaining 24% objects contain extended, core-jet structures, typical of nearby Seyfert galaxies.
3. The detection rate of compact radio structure in NLS1, Seyfert 1 and Seyfert 2 galaxies is consistent with the unified scheme hypothesis.
4. The distributions of radio power for Seyfert 1 along with NLS1 galaxies and Seyfert 2 galaxies for the sample are not significantly different. This is possibly consistent with the unified scheme hypothesis. However, given the size of the sample with several upper limits, it is difficult to uncover any subtle differences that might exist between the types of Seyfert galaxies.
5. There is possibly no evidence of relativistic beaming in nuclei for objects in our sample.
6. Approximately 8% of the sample sources have ratio of radio luminosity and [O III] $\lambda$ 5007 Å luminosity such that they qualify as radio-intermediate sources and the remaining are radio-quiet.
7. The distributions of line luminosities and the X-ray luminosities for the two Seyfert types are also consistent with the unified scheme hypothesis.
8. These sample objects clearly show AGN activities with $\leq$10% contribution from thermal emission, and they show poor ($\sim 0.6\ M_{\odot}\ \mathrm{yr}^{-1}$) SFRs, typical of Seyfert galaxies.
9. It seems that there is ionization stratification associated with clouds, and possibly clouds on scales of 0.1–1.0 kpc have large optical depths at 1.4 GHz, which are responsible for free–free absorption of radio emission from the core, possibly, leading to low radio detection rate for these objects.

However, a weakness remains with the data; these survey images are sensitive to extended emission from starburst activity around the nucleus in addition to the compact emission with the Seyfert core. Future deeper, high-resolution and high-sensitivity radio observations at both, high and low radio frequencies are needed to (i) test and understand the low detection rate, (ii) resolve the FIRST survey images into structures of sizes less than a kiloparsec, (iii) test the predictions of free–free absorption of radio core emission by the narrow-line region clouds, and (iv) understand if these objects have AGN-like, high-brightness temperature flat-spectrum cores, or these have steep-spectrum diffuse emission.

## ACKNOWLEDGMENTS

The author thanks the anonymous referee for suggestions and criticisms which improved the paper. He also thanks Prof. M. Elvis and Prof. M.J. Ward for many helpful conversations, and Dr. M.J. Hardcastle and Dr. D.A. Green for a careful reading of this manuscript. The VLA is operated by the US National Radio Astronomy Observatory which is operated by Associated Universities, Inc., under cooperative agreement with the National Science Foundation. The National Radio Astronomy Observatory is a facility of the National Science Foundation operated under cooperative agreement by Associated Universities, Inc. This research has made use of the NASA/IPAC Extragalactic Database (NED) which is operated by the Jet Propulsion Laboratory, California Institute of Technology, under contract with NASA.

## REFERENCES

Alonso-Herrero, A., Pereira-Santaella, M., Rieke, G. H., Diamond-Stanic, A. M., Wang, Y., Hernán-Caballero, A., & Rigopoulou, D. 2013, Local Luminous Infrared Galaxies. III. Co-evolution of Black Hole Growth and Star Formation Activity?, ApJ, 765, 78

Antonucci, R. R. J. 1993, Unified Models for Active Galactic Nuclei and Quasars, ARAA, 31, 473

Baum, S. A., & Heckman, T. 1989, Extended Opti-

cal Line Emitting Gas in Powerful Radio Galaxies - Statistical Properties and Physical Conditions, ApJ, 336, 681
Becker, R. H, White, R. L., Helfand, & D. J. 1995, The FIRST Survey: Faint Images of the Radio Sky at Twenty Centimeters, ApJ, 450, 559
Bell, E. F. 2003, Estimating Star Formation Rates from Infrared and Radio Luminosities: The Origin of the Radio-Infrared Correlation, ApJ, 586, 794
Boller, T. 2000, ROSAT Results on Narrow-Line Seyfert 1 Galaxies, New Astron. Rev., 44, 387
Broderick, J. W., & Fender, R. P. 2011, Is There Really a Dichotomy in Active Galactic Nucleus Jet Power?, MNRAS, 417, 184
Cappi, M., Panessa, F., Bassani, L., et al. 2006, X-Ray Spectral Survey with XMM-Newton of a Complete Sample of Nearby Seyfert Galaxies, A&A, 446, 459
Colbert, E. J. M., Baum, S. A., Gallimore, J. F., O'Dea, C. P., & Christensen, J. A. 1996a, Large-Scale Outflows in Edge-on Seyfert Galaxies. II. Kiloparsec-Scale Radio Continuum Emission, ApJ, 467, 551
Colbert, E. J. M., Baum, S. A., Gallimore, J. F., O'Dea, C. P., Lehnert, M. D., Tsvetanov, Z. I., Mulchaey, J. S., & Caganoff, S. 1996b, Large-Scale Outflows in Edge-on Seyfert Galaxies. I. Optical Emission-Line Imaging and Optical Spectroscopy, ApJS, 105, 75
Condon, J. J., Cotton, W. D., Greisen, E. W., Yin, Q. F., Perley, R. A., Taylor, G. B., & Broderick, J. J. 1998, The NRAO VLA Sky Survey, AJ, 115, 1693
Dadina, M. 2008, Seyfert Galaxies in the Local Universe ($z \leq 0.1$): the Average X-Ray Spectrum as Seen by BeppoSAX, A&A, 485, 417
Deo, R. P., Crenshaw, D. M., Kraemer, S. B., Dietrich, M., Elitzur, M., Teplitz, H., & Turner, T. J. 2007, Spitzer IRS Observations of Seyfert 1.8 and 1.9 Galaxies: A Comparison with Seyfert 1 and Seyfert 2, ApJ, 671,124
De Robertis, M. M., Osterbrock, D. E., 1984, An Analysis of the Narrow-Line Profiles in High Ionization Seyfert Galaxies, ApJ, 286, 171
Erkens, U., Appenzeller, I., & Wagner, S. 1997, The Nature of the FHIL Winds from AGN, A&A, 323, 707
Evans, I. N., Ford, H. C., Kinney, A. L., Antonucci, A. J., Armus, L., & Caganoff, S. 1991, HST Imaging of the Inner 3 arcseconds of NGC 1068 in the Light of Forbidden [O III] 5007 Å, ApJ, 369, L27
Falcke, H., Sherwood, W., & Patnaik, A. R. 1996, The Nature of Radio-Intermediate Quasars: What Is Radio-Loud and What Is Radio-Quiet?, ApJ, 471, 106
Falcke, H., Wilson, A. S., & Simpson, C. 1998, Hubble Space Telescope and VLA Observations of Seyfert 2 Galaxies: The Relationship between Radio Ejecta and the Narrow-Line Region, ApJ, 502, 199
Gelbord, J. M., Mullaney, J. R., & Ward, M. J. 2009, AGN with Strong Forbidden High-Ionization Lines Selected from the Sloan Digital Sky Survey, MNRAS, 397, 172 (GMW09)
Giuricin, G., Mardirossian, F. Mezzetti, M., & Bertotti, G. 1990, The Radio Properties of Bright Seyfert Galaxies, ApJSS, 72, 551
Gu, Q., Melnick, J., Cid Fernandes, R., Kunth, D., Terlevich, E., & Terlevich, R. 2006, Emission-Line Properties of Seyfert 2 Nuclei, MNRAS, 366, 480
Heckman, T. M., Ptak, A., Hornschemeier, A., & Kauffmann, G. 2005, The Relationship of Hard X-Ray and Optical Line Emission in Low-Redshift Active Galactic Nuclei, ApJ, 634, 161
Ho, L. C. 2005, [O II] Emission in Quasar Host Galaxies: Evidence for a Suppressed Star Formation Efficiency, ApJ, 629, 680
Ho, L. C. 2008, Nuclear Activity in Nearby Galaxies, ARAA, 46, 475
Ho, L. C., & Ulvestad, J. S. 2001, Radio Continuum Survey of an Optically Selected Sample of Nearby Seyfert Galaxies, ApJS, 133, 77
Huchra, J., & Burg, R. 1992, The Spatial Distribution of Active Galactic Nuclei. I - The Density of Seyfert Galaxies and Liners, ApJ, 393, 90
Hunt, L. K., & Malkan, M. A. 1999, Morphology of the 12 Micron Seyfert Galaxies. I. Hubble Types, Axial Ratios, Bars, and Rings, ApJ, 516, 660
Kellermann, K. I., & Owen, F. N. 1988, Radio Galaxies and Quasars, in Springer-Verlag, Galactic and Extragalactic Radio Astronomy, eds. G. L. Verschuur & K. I. Kellermann, 563
Khachikian, E. Y., & Weedman, D. W. 1974, An Atlas of Seyfert Galaxies, ApJ, 192, 581
Kharb, P., Hota, A., Croston, J. H., Hardcastle, M. J., O'Dea, C. P., Kraft, R. P., Axon, D. J., & Robinson, A. 2010, Parsec-Scale Imaging of the Radio-Bubble Seyfert Galaxy NGC 6764, ApJ, 723, 580
Komossa, S., Xu, D., Zhou, H., Storchi-Bergmann, T., & Binette, L. 2008, On the Nature of Seyfert Galaxies with High [O III] $\lambda$5007 Blueshifts, ApJ, 680, 926
Koski, A. T. 1978, Spectrophotometry of Seyfert 2 Galaxies and Narrow-Line Radio Galaxies, ApJ, 223, 56
Kruper, J. S., Canizares, C. R., & Urry, C. M. 1990, Soft X-Ray Properties of Seyfert Galaxies. I - Spectra, ApJS, 74, 347
Kukula, M. J., Pedlar, A., Baum, S. A., & O'Dea, C. P. 1995, High-Resolution Radio Observations of the CfA Seyfert Sample - I. The Observations, MNRAS, 276, 1262
Laing, R., Riley, J. M., & Longair, M. S. 1983, Bright Radio Sources at 178 MHz - Flux Densities, Optical Identifications and the Cosmological Evolution of Powerful Radio Galaxies, MNRAS, 204, 151
Lal, D. V., & Ho, L. C. 2010, The Radio Properties of Type 2 Quasars, AJ, 139, 1089
Lal, D. V., & Rao, A. P. 2007, Giant Metrewave Radio Telescope Observations of X-Shaped Radio Sources, MNRAS, 374, 1085
Lal, D. V., Shastri, P., & Gabuzda, D. C. 2004, Milliarcsec-Scale Radio Structure of a Matched Sample of Seyfert 1 and Seyfert 2 Galaxies, A&A, 425, 99
Lal, D. V., Shastri, P., & Gabuzda, D. C. 2011, Seyfert

Galaxies: Nuclear Radio Structure and Unification, ApJ, 731, 68
Liu, X., Zakamska, N. L., Greene, J. E., Strauss, M. A., Krolik, J. H., & Heckman, T. M. 2009, Host Galaxies of Luminous Type 2 Quasars at $z$ ∼0.5, ApJ, 702, 1098
Mainieri, V., Rigopoulou, D., Lehmann, I., Scott, S., Matute, I., Almaini, O., Tozzi, P., Hasinger, G., & Dunlop, J. S. 2005, Submillimetre Detection of a High-Redshift Type 2 QSO, MNRAS, 356, 1571
Martínez-Sansigre, A., Rawlings, S., Garn, T., Green, D. A., Alexander, P., Klöckner, H.-R., & Riley, J. M. 2006, A Population of High-Redshift Type 2 Quasars - II. Radio Properties, MNRAS, 373, L80
Mas-Hesse, J. M., Rodriguez-Pascual, P. M., de Cordoba, L. S. F., & Mirabel, I. F. 1994, Multiwavelength Analysis of Quasars, Seyfert Galaxies, and Starbursts, ApJS, 92, 599
Mason, R. E., Lopez-Rodriguez E., Packham, C., et al. 2012, The Nuclear Infrared Emission of Low-luminosity Active Galactic Nuclei, AJ, 144, 11
Miller, P., Rawlings, S., & Saunders, R. 1993, The Radio and Optical Properties of the $z$ <0.5 BQS Quasars, MNRAS, 263, 425
Murayama, T., & Taniguchi, Y. 1998, Where Is the Coronal Line Region in Active Galactic Nuclei?, ApJ, 497, L9
Mundell, C. G., Ferruit, P., Nagar, N., & Wilson, A. S. 2009, Radio Variability in Seyfert Nuclei, ApJ, 703, 802
Nagao, T., Taniguchi, Y., & Murayama, T. 2000, High-Ionization Nuclear Emission-Line Region of Seyfert Galaxies, AJ, 119, 2605
Netzer, H. 2015, Revisiting the Unified Model of Active Galactic Nuclei, ARA&A, 53, 365
Norris, R. P., Roy, A. L., Allen, D. A., Kesteven, M. J., Truope, E. R., & Reynolds, J. E. 1992, Compact Radio Cores in Seyfert and Starburst Galaxies, in ASP Conf. Ser. 31, Relationships between Active Galactic Nuclei and Starburst Galaxies, ed. Alexie V. Filippenko, 71
Osterbrock, D. E. 1981, Seyfert Galaxies with Weak Broad H alpha Emission Lines, ApJ, 249, 462
Osterbrock, D. E. 1991, Active Galactic Nuclei, Rep. Prog. Phys., 54, 579
Osterbrock, D. E., & Pogge, R. W. 1985, The Spectra of Narrow-Line Seyfert 1 Galaxies, ApJ, 297, 166
Panessa, F., & Giroletti, M. 2013, Sub-Parsec Radio Cores in Nearby Seyfert Galaxies, MNRAS, 432, 1138
Rawlings, S., & Saunders, R. 1991, Evidence for a Common Central-Engine Mechanism in All Extragalactic Radio Sources, Nature, 349, 138
Roy, A. L., Norris, R. P., Kesteven, M. J., Troup, E. R., & Reynolds, J. E. 1994, Compact Radio Cores in Seyfert Galaxies, ApJ, 432, 496
Rosario, D. J., Santini, P., Lutz, D., et al. 2012, The Mean Star Formation Rate of X-Ray Selected Active Galaxies and Its Evolution from $z$ ∼2.5: Results from PEP-Herschel, A&A, 545, 45
Rush, B., Malkan, M. A., & Spinoglio, L. 1993, The Extended 12 micron Galaxy Sample, ApJS, 89, 1
Schmitt, H. R., Antonucci, R. R. J., Ulvestad, J. S., Kinney, A. L., Clarke, C. J., & Pringle, J. E. 2001, Testing the Unified Model with an Infrared-Selected Sample of Seyfert Galaxies, ApJ, 555, 663
Siegel, S., & Castellan, Jr. N. J. 1981, Nonparametric Statistics for the Behavioral Sciences
Singh, V., Shastri, P., Ishwara-Chandra, C. H., & Athreya, R. 2013, Low-Frequency Radio Observations of Seyfert Galaxies: A Test of the Unification Scheme, A&A, 554, 85
Spergel, D. N., Verde, L., Peiris, H. V. E., et al. 2003, First-Year Wilkinson Microwave Anisotropy Probe (WMAP) Observations: Determination of Cosmological Parameters, ApJS, 148, 175
Thean, A., Pedlar, A., Kukula, M. J., Baum, S. A., & O'Dea, C. P. 2000, High-Resolution Radio Observations of Seyfert Galaxies in the Extended 12-$\mu$m Sample - I. The Observations, MNRAS, 314, 573
Thean, A., Pedlar, A., Kukula, M. J., Baum, S. A., & O'Dea, C. P. 2001, High-Resolution Radio Observations of Seyfert Galaxies in the Extended 12-$\mu$m Sample - II. The Properties of Compact Radio Components, MNRAS, 325, 737
Ulvestad, J. S., & Ho, L. C. 2001, Statistical Properties of Radio Emission from the Palomar Seyfert Galaxies, ApJ, 558, 561
Ulvestad, J. S., & Wilson, A. S. 1984, Radio Structures of Seyfert Galaxies. V - A Flux-Limited Sample of Markarian Galaxies, ApJ, 278, 544
Ulvestad, J. S., Wilson, A. S., & Sramek, R. A. 1981, Radio Structures of Seyfert Galaxies. II, ApJ, 247, 419
Urry, C. M., & Padovani, P. 1995, Unified Schemes for Radio-Loud Active Galactic Nuclei, PASP, 107, 803
Veilleux, S. 1988, A Search for Variations of Forbidden Fe VII 6087-Å Lines and Forbidden Fe X 6375-Å Lines in High-Ionization Seyfert Galaxies, AJ, 95, 1695
Valencia-S. M., Zuther, J., Eckart, A., García-Marín, M., Iserlohe, C., & Wright, G. 2012, Is IRAS 01072+4954 a True-Seyfert 2?. Hints from Near-Infrared Integral Field Spectroscopy, A&A, 544, 129
Vignali, C., Pozzi, F., Fritz, J., et al. 2009, The HELLAS2XMM Survey - XII. The Infrared/Submillimetre View of an X-Ray Selected Type 2 Quasar at $z$ ∼2, MNRAS, 395, 2189
Wang, J., Mao, Y. F., & Wei, J. Y. 2009, Accretion Properties of a Sample of Hard X-Ray (<60 keV) Selected Seyfert 1 Galaxies, AJ, 137, 3388
Whittle, M., Haniff, C. A., Ward, M. J., Meurs, E. J. A., Pedlar, A., Unger, S. W., Axon, D. J., & Harrison, B. A. 1986, Extended Forbidden O III Emission Associated with Nuclear Radio Lobes in the Seyfert Galaxy NGC 5929, MNRAS, 222, 186
Xu, C., Livio, M., & Baum, S. A. 1999, Radio-Loud and Radio-Quiet Active Galactic Nuclei, AJ, 118, 1169